

## Research Paper

# Palladium-103 ( $^{103}\text{Pd}/^{103\text{m}}\text{Rh}$ ), a promising Auger-electron emitter for targeted radionuclide therapy of disseminated tumor cells – absorbed doses in single cells and clusters, with comparison to $^{177}\text{Lu}$ and $^{161}\text{Tb}$

Elif Hindié<sup>1,2</sup>✉, Alexandre Larouze<sup>3</sup>, Mario Alcocer-Ávila<sup>3</sup>, Clément Morgat<sup>1</sup>, Christophe Champion<sup>3</sup>✉

1. Service de Médecine Nucléaire, CHU de Bordeaux, Université de Bordeaux, UMR CNRS 5287, INCIA, F-33400, Talence, France.

2. Institut Universitaire de France, 1 rue Descartes, 75231 Paris cedex 05, France.

3. Université de Bordeaux-CNRS-CEA, Centre Lasers Intenses et Applications, UMR 5107, 33405 Talence, France.

✉ Corresponding authors: Prof. Elif Hindié, Nuclear Medicine Department, University Hospitals of Bordeaux, 33604 Pessac, France; Email: elif.hindie@chu-bordeaux.fr; Phone: 00-33-557656786; Fax: 00-33-557656634; <https://orcid.org/0000-0003-2101-5626>. Prof. Christophe Champion: christophe.champion@u-bordeaux.fr.© The author(s). This is an open access article distributed under the terms of the Creative Commons Attribution License (<https://creativecommons.org/licenses/by/4.0/>). See <http://ivyspring.com/terms> for full terms and conditions.

Received: 2024.02.18; Accepted: 2024.07.02; Published: 2024.07.08

## Abstract

Early use of targeted radionuclide therapy (TRT) to eradicate disseminated tumor cells (DTCs) might offer cure. Selection of appropriate radionuclides is required. This work highlights the potential of  $^{103}\text{Pd}$  ( $T_{1/2} = 16.991$  d) which decays to  $^{103\text{m}}\text{Rh}$  ( $T_{1/2} = 56.12$  min) then to stable  $^{103}\text{Rh}$  with emission of Auger and conversion electrons.

**Methods:** The Monte Carlo track structure code CELLDOSE was used to assess absorbed doses in single cells (14- $\mu\text{m}$  diameter; 10- $\mu\text{m}$  nucleus) and clusters of 19 cells. The radionuclide was distributed on the cell surface, within the cytoplasm, or in the nucleus. Absorbed doses from  $^{103}\text{Pd}$ ,  $^{177}\text{Lu}$  and  $^{161}\text{Tb}$  were compared after energy normalization. The impact of non-uniform cell targeting, and the potential benefit from dual-targeting was investigated. Additional results related to  $^{103\text{m}}\text{Rh}$ , if used directly, are provided.

**Results:** In the single cell, and depending on radionuclide distribution,  $^{103}\text{Pd}$  delivered 7- to 10-fold higher nuclear absorbed dose and 9- to 25-fold higher membrane dose than  $^{177}\text{Lu}$ . In the 19-cell clusters,  $^{103}\text{Pd}$  absorbed doses also largely exceeded  $^{177}\text{Lu}$ . In both situations,  $^{161}\text{Tb}$  stood in-between  $^{103}\text{Pd}$  and  $^{177}\text{Lu}$ . Non-uniform targeting, considering four unlabeled cells within the cluster, resulted in moderate-to-severe dose heterogeneity. For example, with intranuclear  $^{103}\text{Pd}$ , unlabeled cells received only 14% of the expected nuclear dose. Targeting with two  $^{103}\text{Pd}$ -labeled radiopharmaceuticals minimized dose heterogeneity.

**Conclusion:**  $^{103}\text{Pd}$ , a next-generation Auger emitter, can deliver substantially higher absorbed doses than  $^{177}\text{Lu}$  to single tumor cells and cell clusters. This may open new horizons for the use of TRT in adjuvant or neoadjuvant settings, or for targeting minimal residual disease.

Keywords: targeted radionuclide therapy (TRT), palladium-103,  $^{103}\text{Pd}$  ( $^{103}\text{Pd}/^{103\text{m}}\text{Rh}$ ), absorbed dose, tumor cells

## Introduction

Targeted radionuclide therapy (TRT) is evolving rapidly [1]. Lutetium-177-labeled radiopharmaceuticals aiming somatostatin receptors in metastatic neuroendocrine tumors ( $^{177}\text{Lu}$ -DOTATATE, lutathera®) or PSMA in castration-resistant metastatic prostate cancer ( $^{177}\text{Lu}$ -PSMA-617, pluvicto®) are now

new standards of care [2, 3], and many other tumor-targeting radiopharmaceuticals are being developed [1]. While TRT in advanced disease mainly offers palliative outcomes, earlier use, for eradicating disseminated tumors cells (DTCs) and occult micrometastases, might offer cure. Ongoing trials in

high-risk prostate cancer, for example, use TRT before surgery [4], or in combination with external beam radiotherapy (NCT05162573). In many cancers, risks of distant relapse can now be predicted based on clinicopathological and genomic features, response to neoadjuvant treatment, presence of circulating tumor cells (CTCs) or circulating tumor DNA, or other biomarkers. Distant metastases start with tumor cells intravasation within bloodstream. Although rare, CTCs clusters can more efficiently resist cell death, evade the immune system, and colonize secondary sites than single CTCs [5, 6]. CTCs that succeed extravasation and homing in bone marrow or other organs may develop or lay dormant before switching to a proliferative state [6, 7].

To be successful in preventing recurrence, TRT should be able to eradicate lesions of various sizes, including occult micrometastases, DTCs, CTCs clusters and single cells. Conventional  $\beta$ -emitters can lose efficacy in tiny lesions [8, 9]. A  $^{177}\text{Lu}$  tissue concentration that delivers 104 Gy in a lesion of 1 mm diameter, would deliver 24.5 Gy in a 100- $\mu\text{m}$  lesion and 3.9 Gy in a 10- $\mu\text{m}$  cell-sized sphere [9]. This might explain resistance to therapy of some thyroid cancer micrometastases [10], or relapses at new bone marrow sites after exceptional responses to  $^{177}\text{Lu}$ -PSMA-617 [11]. The  $\beta$ -emitter terbium-161 ( $^{161}\text{Tb}$ ) showed superiority over  $^{177}\text{Lu}$  [12, 13], leading to clinical trials in advanced cancers (NCT05521412, NCT05359146). Auger electrons (AE) and conversion electrons (CE) from  $^{161}\text{Tb}$  can add a boost to targeted cells within metastases [9, 14].  $^{161}\text{Tb}$  can also deliver higher doses than  $^{177}\text{Lu}$  in single cells and clusters [15, 16]. Still, most of the energy carried by  $\beta$ -particles would escape. Therefore, in patients without overt metastases, radionuclides without concomitant  $\beta$ -emission could be more suitable. AE-emitters have attracted increasing attention [17-19]. They emit AE when decaying by electron capture, or CE plus AE after isomeric transition, and can deliver high absorbed doses in small lesions [20, 21]. AE-emitting radioligands can be highly radiotoxic when attached to DNA [22]. Other targets also display high sensitivity, such as cell membrane [23, 24], or mitochondria [25]. While the list of AE-emitters is large, many can be limited by unsuitable half-life, high concomitant photon production, or current difficulty in production or radiochemistry [17, 18, 20]. Notably, Bernhardt et al. emphasized that a photon-to-electron energy ratio per decay ( $p/e$ )  $\leq 2$  is required to reduce normal-tissue and whole-body radiation [20]. For example, high photon emission ( $p/e = 11.6$ ) limited the clinical expansion of  $^{111}\text{In}$  TRT [17].

Palladium-103 ( $^{103}\text{Pd}$ ) is one promising AE-emitter [26-30]. When considering  $^{103}\text{Pd}$  for TRT, it is important to note that  $^{103}\text{Pd}$  decays ( $T_{1/2} = 16.991$  d) by electron capture into rhodium-103m ( $^{103\text{m}}\text{Rh}$ ), which in turns decays ( $T_{1/2} = 56.12$  min) through isomeric transition into stable  $^{103}\text{Rh}$ . We use the notation  $^{103}\text{Pd}/(^{103\text{m}}\text{Rh})$  to refer to the complete decay series.  $^{103}\text{Pd}$  is widely used for brachytherapy with low-energy photons, for example as implanted seeds for prostate cancer or ophthalmic plaques for ocular tumors [31, 32]. However,  $^{103}\text{Pd}$  also emits multiple low-energy electrons and the total electron energy per decay (43.5 keV) is higher than that of photon (16.1 keV), with  $p/e = 0.37$  (Table 1). No-carrier-added  $^{103}\text{Pd}$  can be produced in large quantities using cyclotrons, for example through the  $^{103}\text{Rh}(p,n)^{103}\text{Pd}$  reaction [18, 33]. Refined methods of  $^{103}\text{Pd}$  separation from the rhodium solid target are being developed [34]. Production on liquid targets to ease  $^{103}\text{Pd}$  separation for radiopharmaceutical research is also possible [35]. Regarding bioconjugation, there has been some work in the past with the  $\beta$ -emitter  $^{109}\text{Pd}$ , with labeling of antibodies or porphyrins [36, 37]. Recent advances in palladium chelation open new perspectives for the design of  $^{103}\text{Pd}$ -labeled radiopharmaceuticals for TRT [27].

We here used the Monte Carlo code CELLDOSE to assess absorbed doses from  $^{103}\text{Pd}/(^{103\text{m}}\text{Rh})$ , in comparison to  $^{177}\text{Lu}$  and  $^{161}\text{Tb}$ , in single cells and cell clusters, considering various distributions of the radionuclides. Situations of tumor heterogeneity, and the potential benefit of dual-targeting, were also investigated.

## Methods

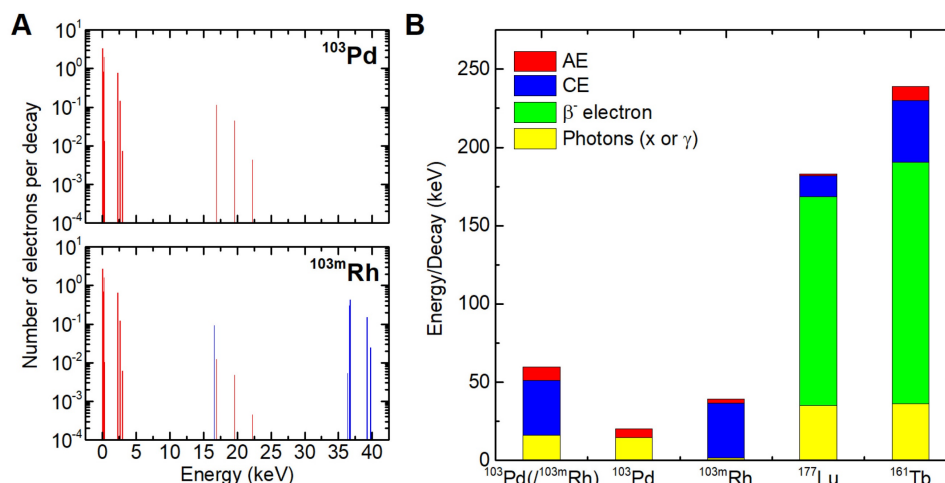
Table 1 and Figure 1 show the main physical characteristics of  $^{103}\text{Pd}/(^{103\text{m}}\text{Rh})$ ,  $^{177}\text{Lu}$  and  $^{161}\text{Tb}$  [38]. As regards  $^{103}\text{Pd}/(^{103\text{m}}\text{Rh})$  electronic emissions, AE ( $^{103}\text{Pd}$  plus  $^{103\text{m}}\text{Rh}$ ) contribute 8.54 keV per decay, and CE ( $^{103\text{m}}\text{Rh}$ ) 34.97 keV.

CELLDOSE is an extension of the Monte Carlo code EPOTRAN, which uses electron cross sections in water that have been extensively verified against experimental data [39]. In a previous work, electronic S-values for iodine-131 with CELLDOSE showed good agreement with data published by Li et al. [8, 40]. In CELLDOSE, energy transfer from an electron to the medium (assimilated to water) is scored event-by-event until its energy falls below 7.4 eV [8]. This allows computing electron absorbed dose down to the nanometer scale [41], as also needed when assessing dose to cell membranes [16].

**Table 1.** Decay characteristics of  $^{103}\text{Pd}/(^{103\text{m}}\text{Rh})$ , its individual parts ( $^{103}\text{Pd}$ ,  $^{103\text{m}}\text{Rh}$ ),  $^{177}\text{Lu}$  and  $^{161}\text{Tb}$ 

Nuclide	$^{103}\text{Pd}/(^{103\text{m}}\text{Rh})$	$^{103}\text{Pd}$	$^{103\text{m}}\text{Rh}$	$^{177}\text{Lu}$	$^{161}\text{Tb}$
Half-life (d)	16.991	16.991	0.039	6.647	6.964
Type of decay	EC / isomeric transition	EC	Isomeric transition	$\beta^-$	$\beta^-$
Daughter	$^{103\text{m}}\text{Rh}$ , then $^{103}\text{Rh}$ stable	$^{103\text{m}}\text{Rh}$ (radioactive)	$^{103}\text{Rh}$ (stable)	$^{177}\text{Hf}$ (stable)	$^{161}\text{Dy}$ (stable)
AE (keV per decay)	8.54	5.82	2.72	1.13	8.94
Number of AE per decay	13.3	7.44	5.88	1.12	11.0
AE energy range in keV (weighted average)*	0.034–22.3 (0.6)	0.034–22.3 (0.8)	0.034–22.3 (0.5)	0.01–61.7 (1)	0.018–50.9 (0.8)
CE (keV per decay)	34.97		34.97	13.52	39.28
CE energy range in keV (weighted average)*	16.6–39.8 (35)		16.6–39.8 (35)	6.2–206 (87)	3.3–98.3 (28)
$\beta$ particles mean energy (keV)				133.3	154.3
Total electron energy per decay (keV)	43.51	5.82	37.69	147.9	202.5
Photons X, $\gamma$ energy per decay (keV)	16.14	14.49	1.65	35.1	36.35
Principal photons: energy domain in keV and (emission probability)	K: 20–23.1 (76.6 %) L: 2.39–3.14 (7.8 %)	K: 20–23.1 (69.3 %) L: 2.69–2.83 (3.68 %)	K: 20–23.1 (7.35 %) L: 2.39–3.14 (4.12 %)	$\gamma$ : 208.4 (11 %) K: 54–65 (5.6 %) L: 7.9–9 (2.5 %)	$\gamma$ : 74.6 (10.2 %) $\gamma$ : 48.9 (17.0 %) K: 45–54 (22.8 %) $\gamma$ : 25.7 (23.2 %) L: 6.4–8.8 (15.2 %)
Total energy per decay in keV (photons + electrons)	59.65	20.31	39.34	183	238.9
Photon/electron energy ratio (p/e)	0.371	2.49	0.044	0.237	0.18

\* The weighted average energy was computed as:  $(\sum_{i=1}^n E_i * w_i) / \sum_{i=1}^n w_i$  where  $w_i$  is the emission probability by nuclear transformation of an electron with energy  $E_i$ .  
EC = electron capture; AE = Auger electrons; CE = conversion electrons

**Figure 1.** Spectra of AE (red) and conversion electrons (CE, blue) from  $^{103}\text{Pd}$  and  $^{103\text{m}}\text{Rh}$  (A). Contribution of photons and various electron categories to energy emitted per decay (B).

First, we studied electron energy deposit around a point source. Next, we computed electron absorbed doses from  $^{103}\text{Pd}/(^{103\text{m}}\text{Rh})$  in spheres with diameters ranging from 1000  $\mu\text{m}$  down to 1  $\mu\text{m}$ , with uniform activity distribution. In CELLDOSE photons are neglected.  $^{103}\text{Pd}/(^{103\text{m}}\text{Rh})$  emits mainly photons in the 20–23 keV domain (76.6% intensity) (Table 1), but also some photons of low energy in the 2.39–3.14 keV domain (7.8% intensity) which can contribute to absorbed dose even in tiny lesions. From NIST database, the half-absorption layer in water for 20 keV photons is  $\sim 12600 \mu\text{m}$ , but for 3 keV photons it is 36  $\mu\text{m}$  (<http://physics.nist.gov/PhysRefData/XrayMassCoef/cover.html>). In order to assess the potential impact of neglecting photons, we computed the photon absorbed dose from  $^{103}\text{Pd}/(^{103\text{m}}\text{Rh})$  in the 1000- $\mu\text{m}$  to 1- $\mu\text{m}$  spheres with uniform activity distribution, taking into account all photon emissions,

using the code PHITS [42].

Because electron energy per decay differs, absorbed doses were assessed for 1 MeV released per  $\mu\text{m}^3$ , meaning 23 decays per  $\mu\text{m}^3$  of  $^{103}\text{Pd}/(^{103\text{m}}\text{Rh})$ , 6.76 decays of  $^{177}\text{Lu}$ , and 4.94 decays of  $^{161}\text{Tb}$ . With this normalization, total energy absorption would theoretically result in 160 Gy [9].

We then assessed nuclear, membrane and cytoplasm electron absorbed doses from  $^{103}\text{Pd}/(^{103\text{m}}\text{Rh})$ ,  $^{177}\text{Lu}$ , or  $^{161}\text{Tb}$ , in single cells and cell clusters. The cluster model consisted of 19 tumor cells with a central cell, six immediate neighbors, and a second layer of 12 neighbors (Figure 2A). Each cell was 14- $\mu\text{m}$  in diameter, with a 10-nm thick membrane and a 10- $\mu\text{m}$  centered nucleus (Figure 2B). A CTC's size can vary widely with cancer type and method used for CTCs enrichment [43]. In one study of metastatic patients, the median diameter of a CTCs was 13.1,

10.7, and 11.0  $\mu\text{m}$  for breast, prostate and colorectal CTCs, respectively [43]. Cancer cells are often characterized by a relatively large nucleus [44]. In our cell model, the nucleus represents 36% of the cell volume.

The radionuclide was distributed on the cell surface, within the cytoplasm, or in the nucleus, with 1436.8 MeV released per labeled cell ( $1436.8 \mu\text{m}^3$ ). Since the nucleus is the most radiosensitive target, when the radionuclide was within the nucleus only the nuclear absorbed dose was assessed.

To study the impact of heterogeneity, we simulated clusters in which 4 of the 19 cells did not retain  $^{103}\text{Pd}$ , mimicking loss of target expression (cells with black stripes in Figure 2A). We then assessed the ability of dual-targeting to counteract dose heterogeneity. These simulations considered two different  $^{103}\text{Pd}$ -labeled radiopharmaceuticals. For each radiopharmaceutical, labeled and unlabeled cells were randomly selected.

We also investigated the impact of higher scale heterogeneity. Here, the 19-cell cluster was replicated six times to build the multi-cluster tumor model depicted in Figure 3. As shown, one of the clusters was not labeled, while the cells of the other clusters kept  $^{103}\text{Pd}/^{103\text{m}}\text{Rh}$  on their surface. We computed the absorbed dose to the nucleus of the central cell of each

cluster (Figure 3).

Finally, as  $^{103\text{m}}\text{Rh}$  can be produced and used directly [17, 18, 20], with the limitation of a short half-life (56.1 min), absorbed doses specific to  $^{103\text{m}}\text{Rh}$  were also calculated.

## Results

### Electron energy deposit around a point source

Ninety-nine percent of the energy released during the transition of  $^{103}\text{Pd}$  to  $^{103\text{m}}\text{Rh}$  was deposited within a radius of 7.37  $\mu\text{m}$  (R99), while for  $^{103\text{m}}\text{Rh}$  decay, R99 was 25.2  $\mu\text{m}$  (Figure 4). Considering the total electron energy released by  $^{103}\text{Pd}/^{103\text{m}}\text{Rh}$ , R99 was 25.0  $\mu\text{m}$ . For comparison, R99 is 1070  $\mu\text{m}$  for  $^{177}\text{Lu}$  and 1060  $\mu\text{m}$  for  $^{161}\text{Tb}$  [9]. As regards more specifically AE, they may be classified into two main energy groups (Figure 1). The first group, with a total of 6.35 electrons per  $^{103}\text{Pd}/^{103\text{m}}\text{Rh}$  decay, has an average energy of 119 eV and a mean electron penetration range of approximately 6.4 nm (down to the 7.4 eV cut-off of CELLDOSE; thus not considering the range of sub-excitation electrons). The second group, with 0.92 electrons per disintegration, has an average energy of 2325 eV, with a mean penetration range of 146 nm.

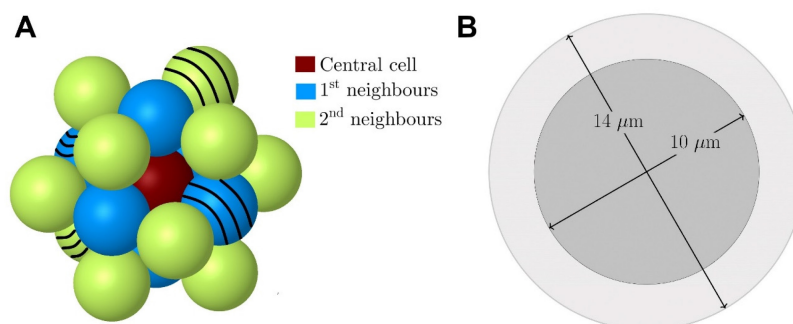


**Figure 2.** Tumor cluster model. In the present study, the cells with the black stripes (4/19) contained no activity. (Adapted from ref-15; Alcocer-Ávila et al.).

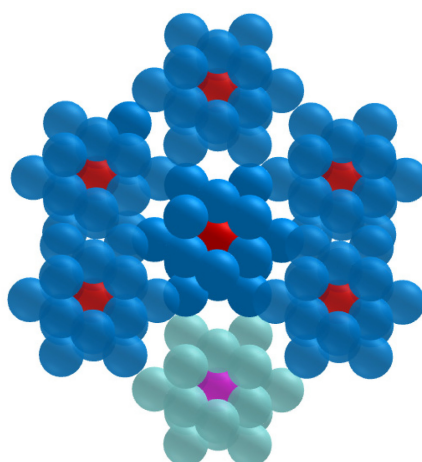


**Figure 3.** Multi-cluster tumor model: The cluster at the bottom of the Figure is unlabeled. The central cell in each cluster is depicted (in red for the six labeled clusters and in pink for the unlabeled cluster).

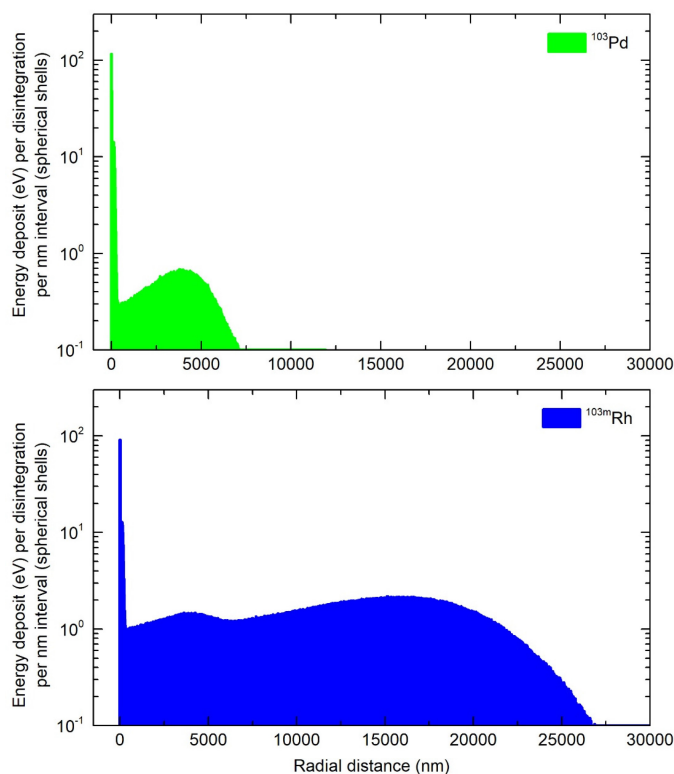


**Figure 4.** Energy deposit within concentric shells of 1-nm thickness per individual decay of <sup>103</sup>Pd (green) and <sup>103m</sup>Rh (blue).

**Table 2.** Electron absorbed doses per decay “S-values” from <sup>103</sup>Pd(/<sup>103m</sup>Rh) and its individual parts (<sup>103</sup>Pd, <sup>103m</sup>Rh) in water spheres of various sizes with homogeneous radionuclide distribution - photon doses and photon-to-electron (p/e) dose ratios are also shown \*

Sphere diameter (μm)	Absorbed dose per decay “S value” in Gy.Bq <sup>-1</sup> .s <sup>-1</sup>			<sup>103</sup> Pd			<sup>103m</sup> Rh		
	<sup>103</sup> Pd(/ <sup>103m</sup> Rh)		p/e dose ratio	Electron	Photon	p/e dose ratio	Electron	Photon	p/e dose ratio
1000	1.31×10 <sup>-8</sup>	2.10×10 <sup>-10</sup>	0.016	1.77×10 <sup>-9</sup>	1.47×10 <sup>-10</sup>	0.083	1.13×10 <sup>-8</sup>	6.23×10 <sup>-11</sup>	0.006
500	1.03×10 <sup>-7</sup>	1.27×10 <sup>-9</sup>	0.012	1.41×10 <sup>-8</sup>	8.28×10 <sup>-10</sup>	0.059	8.86×10 <sup>-8</sup>	4.47×10 <sup>-10</sup>	0.005
200	1.53×10 <sup>-6</sup>	1.50×10 <sup>-8</sup>	0.01	2.18×10 <sup>-7</sup>	9.01×10 <sup>-9</sup>	0.041	1.31×10 <sup>-6</sup>	6.01×10 <sup>-9</sup>	0.005
100	1.12×10 <sup>-5</sup>	9.71×10 <sup>-8</sup>	0.009	1.72×10 <sup>-6</sup>	5.62×10 <sup>-8</sup>	0.033	9.50×10 <sup>-6</sup>	4.09×10 <sup>-8</sup>	0.004
50	7.42×10 <sup>-5</sup>	6.25×10 <sup>-7</sup>	0.008	1.34×10 <sup>-5</sup>	3.55×10 <sup>-7</sup>	0.027	6.08×10 <sup>-5</sup>	2.70×10 <sup>-7</sup>	0.004
20	6.56×10 <sup>-4</sup>	7.67×10 <sup>-6</sup>	0.012	1.92×10 <sup>-4</sup>	4.29×10 <sup>-6</sup>	0.022	4.64×10 <sup>-4</sup>	3.37×10 <sup>-6</sup>	0.007
10	3.39×10 <sup>-3</sup>	5.45×10 <sup>-5</sup>	0.016	1.32×10 <sup>-3</sup>	3.03×10 <sup>-5</sup>	0.023	2.07×10 <sup>-3</sup>	2.42×10 <sup>-5</sup>	0.012
8**				2.41×10 <sup>-3</sup>			3.47×10 <sup>-3</sup>		
5	1.92×10 <sup>-2</sup>	4.06×10 <sup>-4</sup>	0.021	8.52×10 <sup>-3</sup>	2.25×10 <sup>-4</sup>	0.026	1.06×10 <sup>-2</sup>	1.81×10 <sup>-4</sup>	0.017
2	2.26×10 <sup>-1</sup>	6.05×10 <sup>-3</sup>	0.027	1.12×10 <sup>-1</sup>	3.35×10 <sup>-3</sup>	0.03	1.14×10 <sup>-1</sup>	2.71×10 <sup>-3</sup>	0.024
1	1.56×10 <sup>0</sup>	4.76×10 <sup>-2</sup>	0.031	8.08×10 <sup>1</sup>	2.63×10 <sup>-2</sup>	0.033	7.54×10 <sup>1</sup>	2.13×10 <sup>-2</sup>	0.028

\* Electron doses were assessed with CELLDOSE [8]. Photon doses were assessed with PHITS v3.27 [42].

\*\* CELLDOSE electron S-values for the 8μm-sphere are in rather good agreement with electron S-values published by Bolcaen et al. (<sup>103</sup>Pd: 2.21×10<sup>-3</sup> and <sup>103m</sup>Rh: 3.14×10<sup>-3</sup>) [17] using MIRDcell [45].

### Absorbed doses in spheres of various sizes

Table 2 gives electron S-values for <sup>103</sup>Pd(/<sup>103m</sup>Rh) and for individual <sup>103</sup>Pd and <sup>103m</sup>Rh decays. The 8 μm-diameter sphere in Table 2 allows comparison of electronic S-values obtained with CELLDOSE with results published by Bolcaen et al. using the MIRDcell code [17, 45]. S-values obtained with CELLDOSE were in rather good agreement (+8.3% for <sup>103</sup>Pd, +9.5% for <sup>103m</sup>Rh) with those obtained with MIRDcell [17].

Table 2 also shows the photon S-values for <sup>103</sup>Pd(/<sup>103m</sup>Rh) and for individual <sup>103</sup>Pd and <sup>103m</sup>Rh decays. Photon S-values were low compared to electrons, with differences between <sup>103</sup>Pd and <sup>103m</sup>Rh

(<sup>103m</sup>Rh has lower photon emission and, in addition to AE, emits higher energy CE). Considering <sup>103</sup>Pd(/<sup>103m</sup>Rh), the total photon-to-electron (p/e) dose ratio did not exceed 3.1%. Photons were neglected in subsequent simulations.

Table 3 shows normalized electron absorbed doses. Approximately 84% of <sup>103</sup>Pd(/<sup>103m</sup>Rh) electronic energy was retained in a 100 μm-diameter sphere and 25% in a 10 μm-sphere. Normalized electron absorbed doses were higher for <sup>103</sup>Pd(/<sup>103m</sup>Rh) than <sup>177</sup>Lu, with a dose ratio of 5.5 for a 100 μm-sphere and 10.4 for a 10 μm-sphere. The results for <sup>161</sup>Tb were between those of <sup>103</sup>Pd(/<sup>103m</sup>Rh) and <sup>177</sup>Lu (Table 3 and Figure 5).

**Table 3.** Normalized electron absorbed doses in spheres of various sizes with homogeneous radionuclide distribution

Sphere diameter (μm)	Electron absorbed dose for 1 MeV released per μm <sup>3</sup> (Gy) *			Electron dose ratio ( <sup>177</sup> Lu as reference)	
	<sup>103</sup> Pd (/ <sup>103m</sup> Rh)	<sup>177</sup> Lu	<sup>161</sup> Tb	<sup>103</sup> Pd (/ <sup>103m</sup> Rh)	<sup>161</sup> Tb (/ <sup>103m</sup> Rh)
1,000	157	104	108	1.51	1.04
500	154	74.8	82.7	2.07	1.11
200	147	41.8	57.6	3.52	1.38
100	135	24.5	44.5	5.51	1.82
50	112	14.1	33.3	7.91	2.36
20	63.2	6.61	20.2	9.56	3.06
10	40.8	3.92	14.1	10.4	3.60
5	28.8	2.44	9.76	11.8	4.00
2	21.7	1.38	6.74	15.7	4.88
1	18.8	0.88	4.93	21.4	5.60

\* Total absorption corresponds to 160 Gy.

### Electron absorbed doses from <sup>103</sup>Pd(/<sup>103m</sup>Rh), <sup>177</sup>Lu and <sup>161</sup>Tb in the single cell and cell cluster

In the single cell, with 1436.8 MeV released, nuclear absorbed doses with <sup>103</sup>Pd(/<sup>103m</sup>Rh) ranged from 15.6 to 112 Gy, depending on radionuclide location (cell surface, intracytoplasmic or intranuclear), versus 1.93 to 10.7 Gy with <sup>177</sup>Lu, with a dose ratio between 7.8 and 10.5 (Table 4). Considering the dose to the cell membrane, with the radionuclide on the cell surface, the <sup>103</sup>Pd(/<sup>103m</sup>Rh)-to-<sup>177</sup>Lu dose ratio was 25.5 (891 Gy vs. 35 Gy) (Table 4). <sup>161</sup>Tb absorbed doses were between those of <sup>177</sup>Lu and <sup>103</sup>Pd(/<sup>103m</sup>Rh) (Table 4). While AE represent 19.6% of the electron energy released by <sup>103</sup>Pd(/<sup>103m</sup>Rh) (Table 1), they contributed 61% of the nuclear absorbed dose when released within the cell nucleus, and 96% of the

dose to the membrane when the radionuclide was on the cell surface (Table 4). Again, despite representing only 4.4% of the electron energy released by <sup>161</sup>Tb, AE contributed 45% of the nuclear absorbed dose from intranuclear <sup>161</sup>Tb, and 91% of the membrane dose when <sup>161</sup>Tb was on the cell surface (Table 4).

In the 19-cell cluster, nuclear absorbed doses were 7.1 to 9.9-fold higher with <sup>103</sup>Pd(/<sup>103m</sup>Rh) than with <sup>177</sup>Lu, while <sup>161</sup>Tb yielded intermediate values (Table 5). With <sup>103</sup>Pd(/<sup>103m</sup>Rh), <sup>103m</sup>Rh contributed a larger portion of the dose than <sup>103</sup>Pd. Also, self-dose ranged from 26% to 87% with the remaining being cross-dose from surrounding cells.

The results for the single cell and cell cluster are summarized in Figure 6.

### Sensitivity of <sup>103</sup>Pd(/<sup>103m</sup>Rh) to cell-to-cell heterogeneity and investigation of dual-targeting

The impact of non-uniform cell targeting within the 19-cell cluster varies depending on <sup>103</sup>Pd(/<sup>103m</sup>Rh) location (Figure 7). With an intranuclear distribution of <sup>103</sup>Pd(/<sup>103m</sup>Rh), the nuclei of the 4 unlabeled cells received only ~14% of the dose obtained with uniform cell targeting (Figure 7, 1<sup>st</sup> row). With <sup>103</sup>Pd(/<sup>103m</sup>Rh) on the cell surface, the nuclei of the 4 unlabeled cells received ~47% of the dose obtained with uniform cell targeting. In contrast, cell membranes received only ~2.4% of the doses expected with uniform cell targeting (Figure 7, rows 3 and 4).

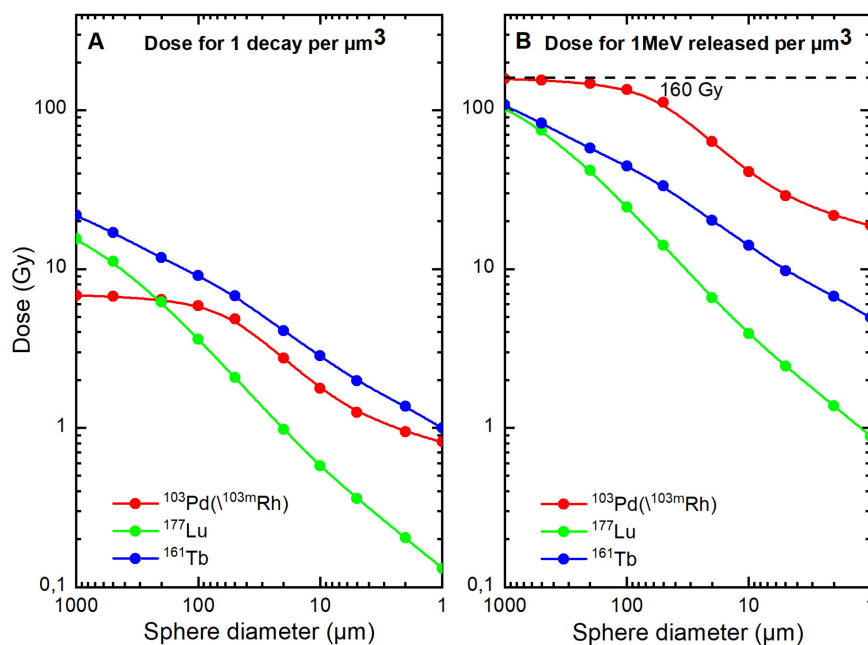


**Figure 5.** Electron absorbed doses from <sup>103</sup>Pd(/<sup>103m</sup>Rh) (red), <sup>177</sup>Lu (green) and <sup>161</sup>Tb (blue), as a function of sphere size. Figure 5A. Dose for 1 decay per μm<sup>3</sup>. Figure 5B. Dose for 1 MeV released per μm<sup>3</sup> (total absorption would lead to 160 Gy).

**Table 4.** Single cell: nuclear, membrane and cytoplasmic absorbed doses from  $^{103}\text{Pd}/(^{103\text{m}}\text{Rh})$ ,  $^{177}\text{Lu}$  and  $^{161}\text{Tb}$ , considering various distributions of the radionuclide \*

	Nuclear absorbed dose (Gy)			Membrane absorbed dose (Gy)		Cytoplasmic absorbed dose (Gy)	
	Radionuclide at cell surface	Radionuclide within cytoplasm	Radionuclide within nucleus	Radionuclide at cell surface	Radionuclide within cytoplasm	Radionuclide at cell surface	Radionuclide within cytoplasm
$^{103}\text{Pd}/(^{103\text{m}}\text{Rh})$	15.6	23.6	112	891	33.9	32.3	58.9
$^{103}\text{Pd}$ dose	2.9	5.2	43.6	478	10.7	9.9	22.5
$^{103\text{m}}\text{Rh}$ dose**	12.7	18.4	68.4	413	23.2	22.4	36.4
AE contribution ( $^{103}\text{Pd} + ^{103\text{m}}\text{Rh}$ )	19.8%	24.3%	61.3%	96.0%	47.2%	45.3%	62.3%
CE contribution ( $^{103\text{m}}\text{Rh}$ )	80.2%	75.7%	38.7%	4.0%	52.8%	54.7%	37.7%
$^{177}\text{Lu}$	1.93	3.01	10.7	35.0	3.68	3.64	5.47
AE contribution	0.44%	3.87%	25.6%	78.3%	18.9%	8.93%	14.0%
$^{161}\text{Tb}$	4.96	8.30	38.6	231	11.6	11.1	19.6
AE contribution	0.66%	6.58%	45.4%	90.8%	36.1%	28.8%	42.2%
<b>Dose ratio <math>^{103}\text{Pd}/(^{103\text{m}}\text{Rh})/^{177}\text{Lu}</math></b>	<b>8.1</b>	<b>7.8</b>	<b>10.5</b>	<b>25.5</b>	<b>9.2</b>	<b>8.9</b>	<b>10.8</b>

\* Normalized absorbed doses for 1436.8 MeV released. With  $^{103}\text{Pd}/(^{103\text{m}}\text{Rh})$ ,  $^{103\text{m}}\text{Rh}$  contributes 1244.6 MeV.

\*\* When  $^{103\text{m}}\text{Rh}$  is used independently, normalized absorbed doses can be derived by multiplying  $^{103\text{m}}\text{Rh}$  figures by 1.154 (1436.8/1244).

**Table 5.** Cluster of 19 cells: electron absorbed doses (Gy) to cell nuclei from  $^{103}\text{Pd}/(^{103\text{m}}\text{Rh})$ , its individual parts ( $^{103}\text{Pd}$ ,  $^{103\text{m}}\text{Rh}$ ),  $^{177}\text{Lu}$ ,  $^{161}\text{Tb}$ , considering various distributions of the radionuclide and cell positions \*

	Cell surface location of the radionuclide N ← CS			Intracytoplasmic location of radionuclide N ← Cy			Intranuclear location of the radionuclide N ← N		
	Central cell	1 <sup>st</sup> neighbors	2 <sup>nd</sup> neighbors	Central cell	1 <sup>st</sup> neighbors	2 <sup>nd</sup> neighbors	Central cell	1 <sup>st</sup> neighbors	2 <sup>nd</sup> neighbors
	$^{103}\text{Pd}/(^{103\text{m}}\text{Rh})$	59.2	45.1	33.4	67.0	52.6	41.2	156	140
(% self-dose)	(26%)	(35%)	(47%)	(35%)	(45%)	(57%)	(72%)	(80%)	(87%)
$^{103}\text{Pd}$ dose	3.8	3.6	3.2	5.8	5.7	5.5	44.2	43	43.4
$^{103\text{m}}\text{Rh}$ dose **	55.4	41.5	30.2	61.2	46.9	35.7	111.8	97	85.6
$^{177}\text{Lu}$	7.20	5.98	4.74	8.26	7.02	5.82	15.7	14.6	13.5
$^{161}\text{Tb}$	15.1	12.4	9.80	17.9	15.3	12.9	47.8	45.2	43.1
<b>Dose-ratio <math>^{103}\text{Pd}/(^{103\text{m}}\text{Rh})/^{177}\text{Lu}</math></b>	<b>8.2</b>	<b>7.5</b>	<b>7.1</b>	<b>8.1</b>	<b>7.5</b>	<b>7.1</b>	<b>9.9</b>	<b>9.6</b>	<b>9.6</b>

\* Normalized absorbed doses considering 1436.8 MeV released per cell. Cells of a given neighborhood receive the same dose (Figure 1).

\*\* When  $^{103\text{m}}\text{Rh}$  is used independently, normalized absorbed doses can be derived by multiplying  $^{103\text{m}}\text{Rh}$  figures by 1.154 (1436.8/1244).

Dual-targeting was mainly beneficial in situations of severe dose heterogeneity. With intranuclear  $^{103}\text{Pd}/(^{103\text{m}}\text{Rh})$  for example, the dose to three of the initially unlabeled cells increased and reached ~50% of the dose expected with uniform cell targeting, while the dose to the fourth cell remained very low, as it stayed untargeted (Figure 7, 1<sup>st</sup> row). With an intracytoplasmic distribution of  $^{103}\text{Pd}/(^{103\text{m}}\text{Rh})$ , the impact of heterogeneity on nuclear absorbed doses was moderate, as well as the benefit from dual-targeting (Figure 7, 2<sup>nd</sup> row). With  $^{103}\text{Pd}/(^{103\text{m}}\text{Rh})$  located on the cell surface, dual-targeting had little impact on nuclear doses, but reduced the heterogeneities in absorbed doses to cell membranes (Figure 7, rows 3 and 4).

**Crossfire from  $^{103}\text{Pd}/(^{103\text{m}}\text{Rh})$  is unable to counter larger spatial heterogeneity**

In the situation illustrated in Figure 3, where one tumor cluster was untargeted while the cells of the other six clusters had  $^{103}\text{Pd}/^{103\text{m}}\text{Rh}$  distributed on their cell surfaces, the nuclear absorbed dose to the central cell of the unlabeled cluster was virtually 0 Gy (Table 6). It is noteworthy that the nucleus of this cell was located 28 μm away from the nearest labeled cells.

**Table 6.** Multi-cluster tumor model (cf. Figure 3): nuclear absorbed doses (Gy) in the central cell of unlabeled and labeled clusters

Absorbed dose [Gy]	Six Labeled Clusters (mean value)	
	Unlabeled cluster	Six Labeled Clusters (mean value)
$^{103}\text{Pd}/(^{103\text{m}}\text{Rh})$	0.00	59.1
$^{177}\text{Lu}$	1.21	8.31
$^{161}\text{Tb}$	0.84	15.8

**Absorbed doses from  $^{103\text{m}}\text{Rh}$  when used directly**

Table 1 and Figures 1 and 4 show  $^{103\text{m}}\text{Rh}$  decay characteristics and profile of energy deposit.  $^{103\text{m}}\text{Rh}$  S-values are listed in Table 2.  $^{103\text{m}}\text{Rh}$  absorbed doses in the single cell and the 19-cell cluster can be derived from data presented in Tables 4 and 5 (see footnotes).

**Discussion**

The present Monte Carlo study aimed at investigating the Auger emitter  $^{103}\text{Pd}/(^{103\text{m}}\text{Rh})$  as candidate radionuclide for TRT. The results highlight the potential of  $^{103}\text{Pd}/(^{103\text{m}}\text{Rh})$  for irradiating single tumor cells and cell clusters. We also show some limitations with  $^{103}\text{Pd}/(^{103\text{m}}\text{Rh})$  in situations of non-uniform targeting. Two radionuclides that we previously assessed,  $^{177}\text{Lu}$  and  $^{161}\text{Tb}$ , were used as

comparators [15]. The  $\beta$ -emitter  $^{177}\text{Lu}$  is widely used for TRT following results with  $^{177}\text{Lu}$ -PSMA-617 and  $^{177}\text{Lu}$ -DOTATATE [2, 3].  $^{161}\text{Tb}$  is a  $\beta$ -emitter that additionally emits CE and AE. It was selected for comparison with  $^{103}\text{Pd}/(^{103\text{m}}\text{Rh})$  because preclinical data suggest its superiority to  $^{177}\text{Lu}$  for small tumor lesions [12, 13]. Clinical trials with  $^{161}\text{Tb}$  have commenced, and this radionuclide is gaining increasing interest within the field [46-48].

From the present Monte Carlo simulations,  $^{103}\text{Pd}/(^{103\text{m}}\text{Rh})$  stands as a highly promising candidate for TRT applications aiming the eradication of DTCs. Whatever the subcellular distribution (cell surface,

intracytoplasmic, or intranuclear),  $^{103}\text{Pd}/(^{103\text{m}}\text{Rh})$  delivered higher nuclear absorbed doses than  $^{177}\text{Lu}$ .  $^{103}\text{Pd}/(^{103\text{m}}\text{Rh})$ -to- $^{177}\text{Lu}$  dose ratios ranged from 7.8 to 10.5 in the single cell and from 7.1 to 9.9 in the 19-cell cluster (Tables 4 and 5 and Figure 6). The absorbed doses for  $^{161}\text{Tb}$  were between those for  $^{103}\text{Pd}/(^{103\text{m}}\text{Rh})$  and  $^{177}\text{Lu}$ . Increasing  $^{177}\text{Lu}$  administered activity can be a means to compensate for lower absorbed dose in single tumor cells and cell clusters. However, this would be associated with increased toxicity, which is not desirable, especially if TRT is given in the adjuvant setting where many patients could never relapse even without treatment.

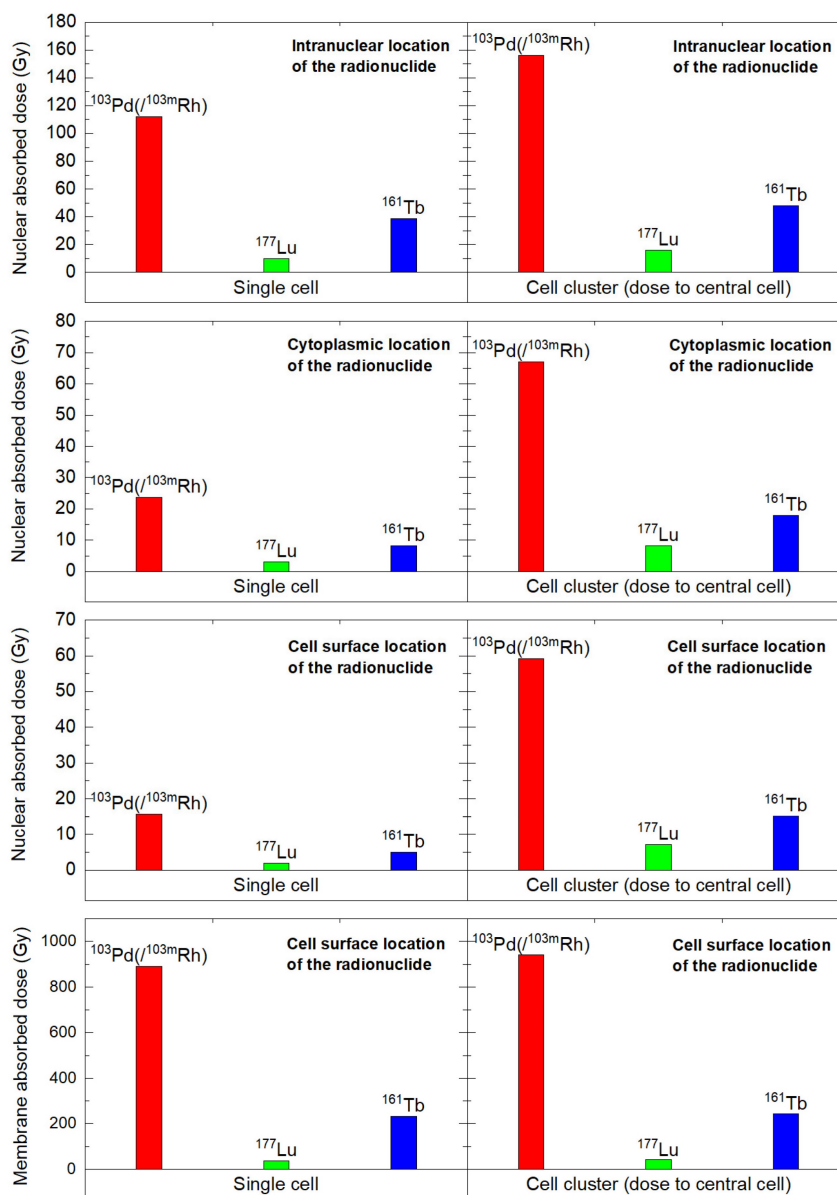


**Figure 6.** Nuclear and membrane absorbed doses to the single cell and central cell of a 19 cells-cluster, considering various distributions of  $^{103}\text{Pd}/(^{103\text{m}}\text{Rh})$  (red),  $^{177}\text{Lu}$  (green), and  $^{161}\text{Tb}$  (blue).

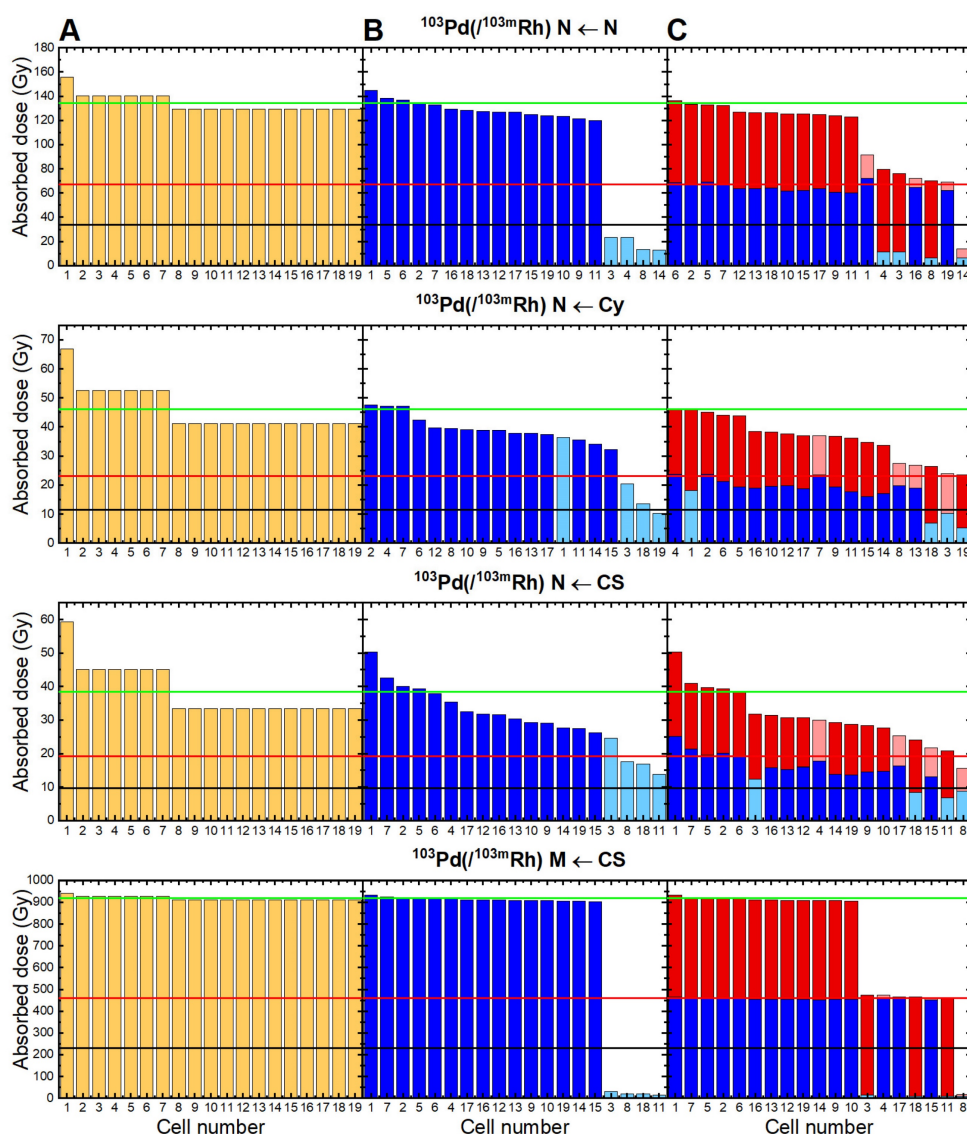


**Figure 7.** Absorbed doses delivered by  $^{103}\text{Pd}/(^{103\text{m}}\text{Rh})$  when all 19 cells in the cluster are targeted (Figure 7A); when 4 cells (in light blue) are not targeted (Figure 7B); with dual-targeting using two  $^{103}\text{Pd}$ -labeled radiopharmaceuticals, each recognizing only 15 cells, and taking the mean of the two Monte Carlo simulations (Figure 7C). With dual-targeting, absorbed doses from first radiopharmaceutical are in blue (light blue representing untargeted cells) and those from second radiopharmaceutical in red (light red for untargeted cells). The green line represents the mean dose with uniform targeting, the red line 50% and the black line 25% of this dose. Cell 1 is central cell, cells 2-7 are first neighbors, and cells 8-19 are second neighbors (cf. Figure 2). N = nuclei; Cy = cytoplasm; CS = cell surface; M = cell membranes.

It would be helpful to convert these results into practical considerations by looking at the number of decays (or also atoms or activity) of  $^{103}\text{Pd}/(^{103\text{m}}\text{Rh})$  versus  $^{177}\text{Lu}$  and  $^{161}\text{Tb}$ , that is needed in the cell to induce lethal damage. We took as reference point the data from O'Neill et al. regarding the CA20948 cell line exposed to  $^{177}\text{Lu}$ -DOTATATE, which indicated that the survival fraction is below 0.01 when the dose to cell nuclei is above 7.3 Gy [49]. Based on the results shown in Table 4 for the simulated 14- $\mu\text{m}$  (1436.8  $\mu\text{m}^3$ ) cell, the number of decays needed to reach a nuclear dose of 7.3 Gy would be, in case of surface distribution: ~15400 decays for  $^{103}\text{Pd}/(^{103\text{m}}\text{Rh})$ , 36700 for  $^{177}\text{Lu}$  and 10400 for  $^{161}\text{Tb}$ ; in case of cytoplasmic distribution: 10200 decays for

$^{103}\text{Pd}/(^{103\text{m}}\text{Rh})$ , 23500 for  $^{177}\text{Lu}$  and 6240 for  $^{161}\text{Tb}$ ; in case of intranuclear location: 2150 decays for  $^{103}\text{Pd}/(^{103\text{m}}\text{Rh})$ , 6630 for  $^{177}\text{Lu}$  and 1340 for  $^{161}\text{Tb}$ .

Also, assuming instant uptake and total disintegration with the radionuclide specific half-life, the initial activity in a cell to reach 7.3 Gy nuclear dose would be, in case of surface distribution: 7.30 mBq  $^{103}\text{Pd}/(^{103\text{m}}\text{Rh})$ , 44.4 mBq  $^{177}\text{Lu}$  or 12.1 mBq  $^{161}\text{Tb}$ ; in case of cytoplasmic distribution: 4.83 mBq  $^{103}\text{Pd}/(^{103\text{m}}\text{Rh})$ , 28.5 mBq  $^{177}\text{Lu}$  or 7.19 mBq  $^{161}\text{Tb}$ ; in case of intranuclear location: 1.02 mBq  $^{103}\text{Pd}/(^{103\text{m}}\text{Rh})$ , 8.00 mBq  $^{177}\text{Lu}$  or 1.55 mBq  $^{161}\text{Tb}$ .

This shows that the required injected activity of  $^{103}\text{Pd}/(^{103\text{m}}\text{Rh})$  could be lower than that of  $^{177}\text{Lu}$ . However, it will be important to ensure that as many

as possible targeting cells would receive  $^{103}\text{Pd}/(^{103\text{m}}\text{Rh})$ , which requires high molar activity (or specific activity) radiopharmaceuticals.

Since many radiopharmaceuticals remain on the cell surface (e.g., neuropeptide antagonist analogs, many antibodies, etc.), the role of cell membrane as target also deserves attention, especially so with AE-emitting radiopharmaceuticals [23, 24]. We previously reported that  $^{161}\text{Tb}$  delivers higher doses to cell membranes than  $^{177}\text{Lu}$  [16]. This is mainly due to AE (Table 4).  $^{161}\text{Tb}$ -labeled somatostatin antagonists, that mostly remain at cell surface, showed high efficacy in a preclinical study [13]. The potential with  $^{103}\text{Pd}/(^{103\text{m}}\text{Rh})$  should be even greater. With  $^{103}\text{Pd}/(^{103\text{m}}\text{Rh})$  located on the cell surface, the cell membrane dose was  $\sim 4$  times higher than with  $^{161}\text{Tb}$ , and  $\sim 25$  times higher than with  $^{177}\text{Lu}$ , with 96% contribution from AE (Table 4, Figure 6). Radiation to cell membrane can lead to cell death [23, 24]. As regards CTCs, it would be interesting to also assess if TRT can influence motility and invasion, or disrupt CTCs clustering.

Heterogeneity in cell uptake/targeting can influence dose distribution [16, 45]. Here, the presence of 4 unlabeled cells within the cluster resulted in marked heterogeneity in nuclear absorbed doses, when  $^{103}\text{Pd}/(^{103\text{m}}\text{Rh})$  was located within cell nuclei, or in absorbed doses to cell membranes, when  $^{103}\text{Pd}/(^{103\text{m}}\text{Rh})$  was on the cell surface (Figure 7). Targeting with two different  $^{103}\text{Pd}$ -labeled radiopharmaceuticals offered some compensation (Figure 7). Multi-targeting is a promising avenue [1]. Understanding target expression and potential heterogeneity of CTCs and DTCs, including dormant and cancer stem cells, would be helpful for designing appropriate single- or dual-targeting TRT strategies in early settings. Derlin and colleagues showed that heterogeneity in PSMA expression was present in early tumor biopsies of prostate cancer, as well as among CTCs in patients with advanced disease. A high proportion of PSMA-negative CTCs was predictive of treatment failure in  $^{177}\text{Lu}$ -PSMA therapy [50].

Advantages and disadvantages of  $^{103}\text{Pd}/(^{103\text{m}}\text{Rh})$  warrant further discussion. Labeling radiopharmaceuticals with the  $^{103}\text{Pd}/(^{103\text{m}}\text{Rh})$  generator allows one to take advantage of the excellent characteristics of  $^{103\text{m}}\text{Rh}$ , notably low photon emission (p/e: 0.044), while circumventing  $^{103\text{m}}\text{Rh}$  short half-life (56.1 min), which is unsuitable for most clinical scenarios. The  $^{103}\text{Pd}/(^{103\text{m}}\text{Rh})$  emission profile, composed of low-energy AE ( $^{103}\text{Pd}$  and  $^{103\text{m}}\text{Rh}$  decays) and medium-energy CE ( $^{103\text{m}}\text{Rh}$ ), is overall remarkable (Figure 1). Also, 99% of  $^{103}\text{Pd}/(^{103\text{m}}\text{Rh})$  electronic energy is deposited within a radius of 25  $\mu\text{m}$ , as

compared with 1070  $\mu\text{m}$  for  $^{177}\text{Lu}$  [9]. This perfectly fits the purpose of targeting single CTCs, CTCs clusters and DTCs. However, cross-dose from  $^{103}\text{Pd}/(^{103\text{m}}\text{Rh})$  is unable to counter larger scale spatial heterogeneity (Figure 3 and Table 6).

Furthermore, chelating strategies will require specific attention, notably as regards the risk of  $^{103\text{m}}\text{Rh}$  release following  $^{103}\text{Pd}$  decay. Release of  $^{103\text{m}}\text{Rh}$  can indeed provide unnecessary toxicity (with 56 min half-life) to healthy tissues as well decreasing therapeutic efficiency to targeted cells. The recoil energy is low compared to alpha emitters, and  $^{103\text{m}}\text{Rh}$  recoil out of the carrier molecule is not expected [26]. However, it is important to note that after-effects (e.g., fragmentation; exciton; thermal wedge; auto-radiolysis) can also occur following emission of AE or CE [18, 51, 52]. Filosofov et al., suggested that for  $^{103}\text{Pd}$  ( $Z = 46$ ), only  $\sim 60\%$  of the daughter radionuclide would remain bound to the chelate complex; but that released  $^{103\text{m}}\text{Rh}$  would have low mobility within the cell [18]. Experimental measurements with  $^{103}\text{Pd}$ -DOTATATE and  $^{103}\text{Pd}$ -Phtalocyanine-TATE, however, showed only  $\sim 10\%$   $^{103\text{m}}\text{Rh}$  release [53]. It will be important to verify that recently proposed palladium chelators [27], not only form a chemically stable complex with  $^{103}\text{Pd}$ , but also retain  $^{103\text{m}}\text{Rh}$  to the highest extent. The fact that both radionuclides belong to the platinum family might facilitate chelating strategies. Nanostructures can also be used as carriers in some applications [29, 30, 54].

$^{103}\text{Pd}/(^{103\text{m}}\text{Rh})$  half-life ( $\sim 17$  d) lays within the 3-to-20 days range suggested as optimal [17]. Also,  $^{103}\text{Pd}$  brachytherapy of prostate cancer is highly efficacious [31, 32].  $^{103}\text{Pd}/(^{103\text{m}}\text{Rh})$  half-life might facilitate the development of radio-immunotherapy by matching with the long half-lives of antibodies, improving the tumor-to-bone marrow ratio. However, low dose rate TRT can be less suitable to tumors with rapid growth [55].  $^{103}\text{Pd}/(^{103\text{m}}\text{Rh})$  low dose rate TRT is expected to offer excellent normal tissue tolerance, and might permit less fractionation compared to the current 4-to-6 cycles schemas with  $^{177}\text{Lu}$ -labeled radiopharmaceuticals [2, 3]. However, the dose to normal tissues (from electrons and photons) will need to be carefully assessed taking into account the specific distribution of the  $^{103}\text{Pd}/(^{103\text{m}}\text{Rh})$ -labeled radiopharmaceutical that is envisioned for TRT.

$^{103}\text{Pd}/(^{103\text{m}}\text{Rh})$  emits only low-energy photons, meaning less issues regarding shielding, radioprotection and isolation. However, this also precludes post-therapy imaging and dosimetry to normal organs. Dosimetry to occult tumor lesions would not have been possible anyway. Research is needed to see which diagnostic radionuclide(s) may

act as companion when selecting patients for neoadjuvant or adjuvant  $^{103}\text{Pd}/(^{103}\text{mRh})$  therapy, based for example on the level of uptake in the primary tumor [4].

Our study has some limitations. In CELLDOSE, photons are neglected. Table 2 shows that for spheres ranging from  $1\mu\text{m}$ - to  $1000\mu\text{m}$ , the p/e dose ratio does not exceed 3.1%. However, photon contribution of  $^{103}\text{Pd}/(^{103}\text{mRh})$  would need to be taken into account when considering absorbed dose to normal tissues, organs and whole-body [56]. In our simulations, we considered that the  $^{103}\text{mRh}$  decay occurs at the same site as the  $^{103}\text{Pd}$  decay. This assumption will require verification for individual radioligands. We therefore also provided individual absorbed doses from  $^{103}\text{Pd}$  and  $^{103}\text{mRh}$ . The data for  $^{103}\text{mRh}$  can also be useful if this radionuclide is directly utilized. We simulated scenarios of homogeneous distribution within the cytoplasm or nucleus; however, we did not simulate situations of radiopharmaceuticals located within mitochondria [25], or linked to DNA. The development of palladium compounds with such characteristics would be an interesting endeavor [57]. AE-emitting radionuclides can be particularly potent when attached to DNA due to the isotropic (4 $\pi$ ) emission of multiple AE from a single decay [41]. It is noteworthy, however, that the  $\sim 7.44$  AE from  $^{103}\text{Pd}$  and  $\sim 5.88$  AE from  $^{103}\text{mRh}$  are released at separate times. Our simulations considered a fixed CTCs cell size of  $14\mu\text{m}$  with a  $10\mu\text{m}$  centered nucleus, and we use it as a starting point to investigate the cellular dosimetry of  $^{103}\text{Pd}/(^{103}\text{mRh})$ . It will be beneficial for future works to investigate different cell sizes and geometries. It will also be important to compare  $^{103}\text{Pd}/(^{103}\text{mRh})$  to other potential Auger emitters [17-19, 58], as well as to alpha emitters [59, 60]. Finally, absorbed dose is only one aspect to consider given the complexity of radiobiological effects associated with TRT. Bystander cytotoxicity and bystander immunity, for example, can reduce the impact of dose heterogeneity [61].

Avenues of combining TRT with immunotherapy, PARP inhibitors, pro-apoptotic drugs, or other agents are being actively investigated [62-64]. The potential synergy between TRT and immunotherapy has been highlighted [62, 63]. This also deserves investigation in early settings, as CTCs may escape the immune system, for example through enhanced expression of PDL-1 [6, 65].

## Conclusion

Results from the present Monte Carlo simulations show that  $^{103}\text{Pd}/(^{103}\text{mRh})$  might be a promising radionuclide for applications aiming eradication of CTCs, disseminated tumor cells and

occult micrometastases. For all cellular distributions,  $^{103}\text{Pd}/(^{103}\text{mRh})$  delivered substantially higher absorbed doses than  $^{177}\text{Lu}$  to single cells and to a cluster of tumor cells. Absorbed doses from  $^{103}\text{Pd}/(^{103}\text{mRh})$  also exceeded those from  $^{161}\text{Tb}$ . If in-vivo studies confirm these findings, clinical trials with  $^{103}\text{Pd}/(^{103}\text{mRh})$  aiming eradication of disseminated tumor cells can be envisioned.

## Abbreviations

TRT: targeted radionuclide therapy;  $^{103}\text{Pd}$ : palladium-103;  $^{103}\text{mRh}$ : rhodium-103; DTC: disseminated tumor cells; CTCs: circulating tumor cells.

## Acknowledgements

We would like to acknowledge helpful discussions with Prof. Jan Rijn Zeevaart, Radiochemistry, The South African Nuclear Energy Corporation, Pelindaba, Hartbeespoort 0240, South Africa.

This study was conducted in the framework of University of Bordeaux IdEx “Investments for the Future” program RRI “NewMOON”.

## Competing Interests

The authors have declared that no competing interest exists.

## References

1. Aboagye EO, Barwick TD, Haberkorn U. Radiotheranostics in oncology: Making precision medicine possible. *CA Cancer J Clin.* 2023;73:255-274.
2. Sartor O, de Bono J, Chi KN, et al. Lutetium-177-PSMA-617 for metastatic castration-resistant prostate cancer. *N Engl J Med.* 2021;385:1091-1103.
3. Strosberg J, El-Haddad G, Wolin E, et al. Phase 3 trial of  $^{177}\text{Lu}$ -dotatate for midgut neuroendocrine tumors. *N Engl J Med.* 2017;376:125-135.
4. Eapen RS, Buteau JP, Jackson P, et al. Administering [ $^{177}\text{Lu}$ ]Lu-PSMA-617 Prior to Radical Prostatectomy in Men with High-risk Localised Prostate Cancer (LuTectomy): A Single-centre, Single-arm, Phase 1/2 Study. *Eur Urol.* 2024;85:217-226.
5. Yamamoto A, Doak AE, Cheung KJ. Orchestration of collective migration and metastasis by tumor cell clusters. *Annu Rev Pathol.* 2023;18:231-256.
6. Ring A, Nguyen-Sträuli BD, Wicki A, Aceto N. Biology, vulnerabilities and clinical applications of circulating tumour cells. *Nat Rev Cancer.* 2023;23:95-111.
7. Risson E, Nobre AR, Maguer-Satta V, Aguirre-Ghiso JA. The current paradigm and challenges ahead for the dormancy of disseminated tumor cells. *Nat Cancer.* 2020;1:672-680.
8. Champion C, Zanotti-Fregonara P, Hindié E. CELLDOSE: a Monte Carlo code to assess electron dose distribution—S values for  $^{131}\text{I}$  in spheres of various sizes. *J Nucl Med.* 2008;49:151-157.
9. Hindié E, Zanotti-Fregonara P, Quinto MA, Morgat C, Champion C. Dose deposits from  $^{90}\text{Y}$ ,  $^{177}\text{Lu}$ ,  $^{111}\text{In}$ , and  $^{161}\text{Tb}$  in micrometastases of various sizes: Implications for radiopharmaceutical therapy. *J Nucl Med.* 2016;57:759-764.
10. Sisson JC, Jamadar DA, Kazerooni EA, Giordano TJ, Carey JE, Spaulding SA. Treatment of micronodular lung metastases of papillary thyroid cancer: are the tumors too small for effective irradiation from radioiodine? *Thyroid.* 1998;8:215-221.
11. Kostos L, et al. Determinants of outcome following PSMA-based radioligand therapy and mechanisms of resistance in patients with metastatic castration-resistant prostate cancer. *Ther Adv Med Oncol.* 2023;15:17588359231179309.

12. Müller C, Umbricht CA, Gracheva N, et al. Terbium-161 for PSMA-targeted radionuclide therapy of prostate cancer. *Eur J Nucl Med Mol Imaging*. 2019;46:1919-1930.
13. Borgna F, Haller S, Rodríguez JMM, et al. Combination of terbium-161 with somatostatin receptor antagonists—a potential paradigm shift for the treatment of neuroendocrine neoplasms. *Eur J Nucl Med Mol Imaging*. 2022;49:1113-1126.
14. Champion C, Quinto MA, Morgat C, Zanotti-Fregonara P, Hindié E. Comparison between three promising  $\beta$ -emitting radionuclides, ( $^{67}\text{Cu}$ ), ( $^{47}\text{Sc}$ ) and ( $^{161}\text{Tb}$ ), with emphasis on doses delivered to minimal residual disease. *Theranostics*. 2016;6:1611-1618.
15. Alcocer-Ávila ME, Ferreira A, Quinto MA, Morgat C, Hindié E, Champion C. Radiation doses from  $^{161}\text{Tb}$  and  $^{177}\text{Lu}$  in single tumour cells and micrometastases. *EJNMMI Phys*. 2020;7:33.
16. Larouze A, Alcocer-Ávila M, Morgat C, Champion C, Hindié E. Membrane and nuclear absorbed doses from  $^{177}\text{Lu}$  and  $^{161}\text{Tb}$  in tumor clusters: effect of cellular heterogeneity and potential benefit of dual targeting—A Monte Carlo study. *J Nucl Med*. 2023;64:1619-1624.
17. Bolcaen J, Gizawy MA, Terry SYA, et al. Marshalling the potential of Auger electron radiopharmaceutical therapy. *J Nucl Med*. 2023;64:1344-1351.
18. Filosofov D, Kurakina E, Radchenko V. Potent candidates for targeted Auger therapy: production and radiochemical considerations. *Nucl Med Biol*. 2021;94-95:1-19.
19. Ku A, Facca VJ, Cai Z, Reilly RM. Auger electrons for cancer therapy - a review. *EJNMMI Radiopharm Chem*. 2019;4:27.
20. Bernhardt P, Forsell-Aronsson E, Jacobsson L, Skarnemark G. Low-energy electron emitters for targeted radiotherapy of small tumours. *Acta Oncol*. 2001;40:602-608.
21. Falzone N, Fernández-Varea JM, Flux G, Vallis KA. Monte Carlo evaluation of Auger electron-emitting theranostic radionuclides. *J Nucl Med*. 2015;56:1441-1446.
22. Kassis AI. Molecular and cellular radiobiological effects of Auger emitting radionuclides. *Radiat Prot Dosimetry*. 2011;143:241-247.
23. Pouget JP, Santoro L, Raymond L, et al. Cell membrane is a more sensitive target than cytoplasm to dose ionization produced by Auger electrons. *Radiat Res*. 2008;170:192-200.
24. Paillas S, Ladjohounlou R, Lozza C, et al. Localized irradiation of cell membrane by Auger electrons is cytotoxic through oxidative stress-mediated nontargeted effects. *Antioxid Redox Signal*. 2016;25:467-484.
25. Santos JF, Braz MT, Raposinho P, et al. Synthesis and Preclinical Evaluation of PSMA-Targeted  $^{111}\text{In}$ -Radioconjugates Containing a Mitochondria-Tropic Triphenylphosphonium Carrier. *Mol Pharm*. 2024;21:216-233.
26. van Rooyen J, Szucs Z, Zeevaert JR. A possible in vivo generator  $^{103}\text{Pd}/^{103}\text{mRh}$ -recoil considerations. *Appl Radiat Isot*. 2008;66:1346-1349.
27. Pineau J, Lima LMP, Platas-Iglesias C, et al. Relevance of palladium to radiopharmaceutical development considering enhanced coordination properties of TEIPA. *Chemistry*. 2022;28:e202200942.
28. Prasanth Annamalaisamy G, Lyczko M, Bilewicz A. Preparation and characterization of palladium-103/109 bisphosphonate - 2,2' bipyridyl complexes for the treatment of bone cancer metastasis - Preliminary Studies. International Symposium on Trends in Radiopharmaceuticals (ISTR-2023). Book of Abstracts - IAEA-CN-310/129, p 92-92.
29. Gharibkandi NA. Bioconjugates of  $^{103}\text{Pd}/^{103}\text{mRh}$  in-vivo generator for targeted Auger electron therapy. International Symposium on Trends in Radiopharmaceuticals (ISTR-2023). Book of Abstracts - IAEA-CN-310/115, p 81-81.
30. Gandidzanwa S, Beukes N, Joseph SV, et al. The development of folate-functionalised palladium nanoparticles for folate receptor targeting in breast cancer cells. *Nanotechnology*. 2023;34(46). doi: 10.1088/1361-6528/accc52.
31. Tang C, Sanders J, Thames H, et al. Outcomes after PD-103 versus I-125 for low dose rate prostate brachytherapy monotherapy: An international, multi-institutional study. *Radiother Oncol*. 2023;183:109599.
32. Michalski JM, Winter KA, Prestidge BR, et al. Effect of brachytherapy with external beam radiation therapy versus brachytherapy alone for intermediate-risk prostate cancer: NRG Oncology RTOG 0232 randomized clinical trial. *J Clin Oncol*. 2023;41:4035-4044.
33. Hussain M, Sudar S, Aslam MN, et al. A comprehensive evaluation of charged-particle data for production of the therapeutic radionuclide ( $^{103}\text{Pd}$ ). *Appl Radiat Isot*. 2009;67:1842-1854.
34. Laouameria AN, Hunyadi M, Csík A, Szucs Z. Innovative Approach to Producing Palladium-103 for Auger-Emitting Radionuclide Therapy: A Proof-of-Concept Study. *Pharmaceuticals (Basel)*. 2024;17:253.
35. Krol V, Koers LMG, McNeil S, Hoehr C, Radchenko V. Cyclotron production of  $^{103}\text{Pd}$  using a liquid target. *Nucl Med Biol*. 2023;118-119:108328.
36. Fawwaz RA, Wang TS, Srivastava SC, et al. Potential of palladium-109-labeled antimelanoma monoclonal antibody for tumor therapy. *J Nucl Med*. 1984;25:796-799.
37. Das T, Chakraborty S, Sarma HD, Banerjee S. A novel [ $^{109}\text{Pd}$ ] palladium labeled porphyrin for possible use in targeted radiotherapy. *Radiochim Acta*. 2008;96:427-433.
38. Eckerman K, Endo A. ICRP publication 107. Nuclear decay data for dosimetric calculations. *Ann ICRP*. 2008;38:7-96.
39. Champion C, Le Loirec C, Stosic B. EPOTRAN: a full-differential Monte Carlo code for electron and positron transport in liquid and gaseous water. *Int J Radiat Biol*. 2012;88:54-61.
40. Li WB, Friedland W, Pomplun E, et al. Track structures and dose distributions from decays of ( $^{131}\text{I}$ ) and ( $^{125}\text{I}$ ) in and around water spheres simulating micrometastases of differentiated thyroid cancer. *Radiat Res*. 2001;156:419-29.
41. Alcocer Ávila ME, Hindié E, Champion C. How to explain the sensitivity of DNA double-strand breaks yield to 125I position? *Int J Radiat Biol*. 2023;99:103-108.
42. Sato T, Iwamoto Y, Hashimoto S, et al. Recent improvements of the particle and heavy ion transport code system - PHITS Version 3.33. *J Nucl Sci Technol*. 2024;61:127-135.
43. Coumans FA, van Dalum G, Beck M, Terstappen LW. Filter characteristics influencing circulating tumor cell enrichment from whole blood. *PLoS One*. 2013;8:e61770.
44. Jevtić P, Edens LJ, Vuković LD, Levy DL. Sizing and shaping the nucleus: mechanisms and significance. *Curr Opin Cell Biol*. 2014;28:16-27.
45. Katugampola S, Wang J, Rosen A, Howell RW. MIRD pamphlet No. 27: MIRDcell V3, a revised software tool for multicellular dosimetry and bioeffect modeling. *J Nucl Med*. 2022;63:1441-1449.
46. Emmerson B, McIntosh L, Buteau JP, et al. Radiation absorbed dose in patients with metastatic castration-resistant prostate cancer treated with [ $^{161}\text{Tb}$ ] Tb-PSMA-I&T: first results of the VIOLET phase I/II study. *Eur J Nucl Med Mol Imaging*. 2023;50(Suppl 1):S189.
47. Schaefer-Schuler A, Burgard C, Blickle A, et al. [ $^{161}\text{Tb}$ ]Tb-PSMA-617 radioligand therapy in patients with mCRPC: preliminary dosimetry results and intra-individual head-to-head comparison to [ $^{177}\text{Lu}$ ]Lu-PSMA-617. *Theranostics*. 2024;14:1829-1840.
48. Fricke J, Westerbergh F, McDougall L, et al. First-in-human administration of terbium-161-labelled somatostatin receptor subtype 2 antagonist ([ $^{161}\text{Tb}$ ]Tb-DOTA-LM3) in a patient with a metastatic neuroendocrine tumour of the ileum. *Eur J Nucl Med Mol Imaging*. 2024;51:2517-2519.
49. O'Neill E, Kersemans V, Allen PD, et al. Imaging DNA Damage Repair In Vivo After  $^{177}\text{Lu}$ -DOTATATE Therapy. *J Nucl Med*. 2020;61:743-750.
50. Derlin T, Riethdorf S, Schumacher U, et al. PSMA-heterogeneity in metastatic castration-resistant prostate cancer: Circulating tumor cells, metastatic tumor burden, and response to targeted radioligand therapy. *Prostate*. 2023;83:1076-1088.
51. Kurakina ES, Wharton L, Khushvaktov J, Magomedbekov EP, Radchenko V, Filosofov D. Separation of  $^{44}\text{mSc}/^{44}\text{gSc}$  Nuclear Isomers Based on After-Effects. *Inorg Chem*. 2023;62:20646-20654.
52. Mirzadeh S, Kumar K, Gansow OA. The Chemical Fate of  $^{212}\text{Bi}$ -DOTA Formed by  $\beta$ -Decay of  $^{212}\text{Pb}$ (DOTA) $_2$ . *Radiochimica Acta* 1993;60:1-10.
53. Zeevaert JR. Mitigation of the inherent risk posed by the release of a daughter radioisotope in the case of Auger emitting radionuclides. Oral presentation - 10th International Symposium on the Physical, molecular, Cellular and Medical Aspects of Auger Electron Processes - Sept. 8-6 2023, Montpellier, France.
54. Reilly RM, Georgiou CJ, Brown MK, Cai Z. Radiation nanomedicines for cancer treatment: a scientific journey and view of the landscape. *EJNMMI Radiopharm Chem*. 2024;9:37.
55. Dale RG. Dose-rate effects in targeted radiotherapy. *Phys Med Biol*. 1996;41:1871-1884.
56. Dalvand S, Sadeghi M. Bone marrow dosimetry for  $^{141}\text{Ce}$ -EDTMP as a potential bone pain palliation complex: A Monte Carlo study. *Appl Radiat Isot*. 2022;182:110113.
57. Dorafshan Tabatabai AS, Dehghanian E, Mansouri-Torshizi H, Feizi-Dehnyayebi M. Computational and experimental examinations of new antitumor palladium(II) complex: CT-DNA-/BSA-binding, in-silico prediction, DFT perspective, docking, molecular dynamics simulation and ONIOM. *J Biomol Struct Dyn*. 2024;42:5447-5469.
58. Bastami H, Chiniforush TA, Heidari S, Sadeghi M. Dose evaluation of Auger electrons emitted from the  $^{119}\text{Sb}$  in cancer treatment. *Appl Radiat Isot*. 2022;185:110250.

59. Song H, Sgouros G. Alpha and Beta Radiation for Theragnostics. *PET Clin.* 2024;19:307-323.
60. Alcocer-Ávila ME, Larouze A, Groetz JE, Hindíé E, Champion C. Physics and small-scale dosimetry of  $\alpha$  -emitters for targeted radionuclide therapy: The case of  $^{211}\text{At}$ . *Med Phys.* 2024 Mar 13. doi: 10.1002/mp.17016. Online ahead of print.
61. Pouget JP, Santoro L, Piron B, et al. From the target cell theory to a more integrated view of radiobiology in Targeted radionuclide therapy: The Montpellier group's experience. *Nucl Med Biol.* 2022;104-105:53-64.
62. Aggarwal R, Starzinski S, de Kouchkovsky I, et al. Single-dose  $^{177}\text{Lu}$ -PSMA-617 followed by maintenance pembrolizumab in patients with metastatic castration-resistant prostate cancer: an open-label, dose-expansion, phase 1 trial. *Lancet Oncol.* 2023;24:1266-1276.
63. Pouget JP, Chan TA, Galluzzi L, Constanzo J. Radiopharmaceuticals as combinatorial partners for immune checkpoint inhibitors. *Trends Cancer.* 2023;9:968-981.
64. Sandhu S, Joshua AM, Emmett L, et al. LuPARP: Phase 1 trial of  $^{177}\text{Lu}$ -PSMA-617 and olaparib in patients with metastatic castration resistant prostate cancer (mCRPC). *J Clin Oncol.* 2023;41(no. 16\_suppl):5005-5005.
65. Rzhvskiy A, Kapitannikova A, Malinina P, et al. Emerging role of circulating tumor cells in immunotherapy. *Theranostics.* 2021;11:8057-8075.